# ISBI 2011 Overview
# CS Imaging

# COMPRESSIVE SENSING MRI WITH LAPLACIAN SPARSIFYING TRANSFORM

*Ying Dong and Jim Ji*

Department of Electrical & Computer Engineering, Texas A&M University

$$\min TV(x) \quad \text{subject to} \quad b = Ax \qquad (1)$$

where

$$TV(x) := \sum_{ij} \sqrt{(D_{h;ij}x)^2 + (D_{v;ij}x)^2}\ ,$$

$$D_{h;ij}x = \begin{cases} x_{i+1,j} - x_{ij} & i < n \\ 0 & i = n \end{cases}, \qquad D_{v;ij}x = \begin{cases} x_{i,j+1} - x_{ij} & j < n \\ 0 & j = n \end{cases}.$$

$$\min LP(x) \quad \text{subject to} \quad b = Ax$$

where

$$LP(x) := \sum_{ij} \sqrt{(L_{h;ij}x)^2 + (L_{v;ij}x)^2}\ ,$$

$$L_{h;ij}x = \begin{cases} x_{i+1,j} + x_{i-1,j} - 2x_{ij} & 1 < i < n \\ 0 & i = 1, n \end{cases},$$

$$L_{v;ij}x = \begin{cases} x_{i,j+1} + x_{i,j-1} - 2x_{ij} & 1 < j < n \\ 0 & j = 1, n \end{cases}.$$

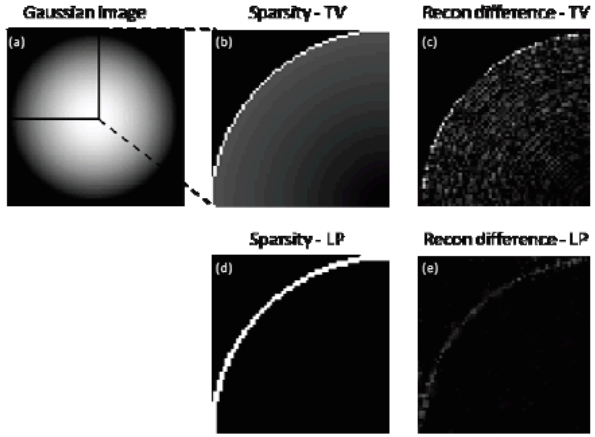


Fig.1 Comparison of the LP minimization and the TV minimization using the simulated 128*128 image: (a) original image with Gaussian variation; (b) the image after sparsifying transform using TV; (c) the reconstruction difference using TV; (d) the image after sparsifying transform using LP; and (e) the reconstruction difference using the proposed LP minimization.

The minimization problem can be recast as a second-order cone program (SOCP),

$$\min_x \sum_{ij} l_{ij} \quad \text{s.t.} \ \left\|\nabla^2 x\right\| \le l_{ij} \ \text{and} \ Ax = b \qquad (3)$$

Then the second-order conic function is defined as

$$f_{l_{ij}} = \frac{1}{2}\left(\left\|\nabla^2 x\right\|_2^2 - l_{ij}^{\ 2}\right) \quad i, j = 1, \ldots, n \qquad (4)$$

(4) can be solved with a generic log-barrier algorithm such as the one being used in $L_1$-magic [4, 6].

performing FFT and extracting the radial lines in k-space. Totally 30 radial lines, which is 21.8% of full k-space data, are used to reconstruct the image.

Additional, a set of 64*64 images are simulated with noise to test the performance. The number of radial k-space lines is 20 (28.3%) and 40 (51.6%), respectively. Both TV and LP minimization are applied in the CS-MRI to reconstruct images. To quantitatively compare the two methods, the normalized mean squared error (NMSE), computational time and signal-to-noise ratio (SNR) of the

Table 1 Quantitative comparison of the proposed LP minimization and the TV minimization

| Prjs | Data % | Method | NMSE | Time (s) | SNR |
|---|---|---|---|---|---|
| 20 | 28.3% | TV | $2.5*10^{-4}$ | 38 | 116 |
| | | LP | $4.4*10^{-4}$ | 61 | 147 |
| 40 | 51.6% | TV | $9.2*10^{-5}$ | 34 | 99 |
| | | LP | $9.4*10^{-5}$ | 43 | 118 |

higher SNR. In addition, the proposed method takes longer reconstruction time.

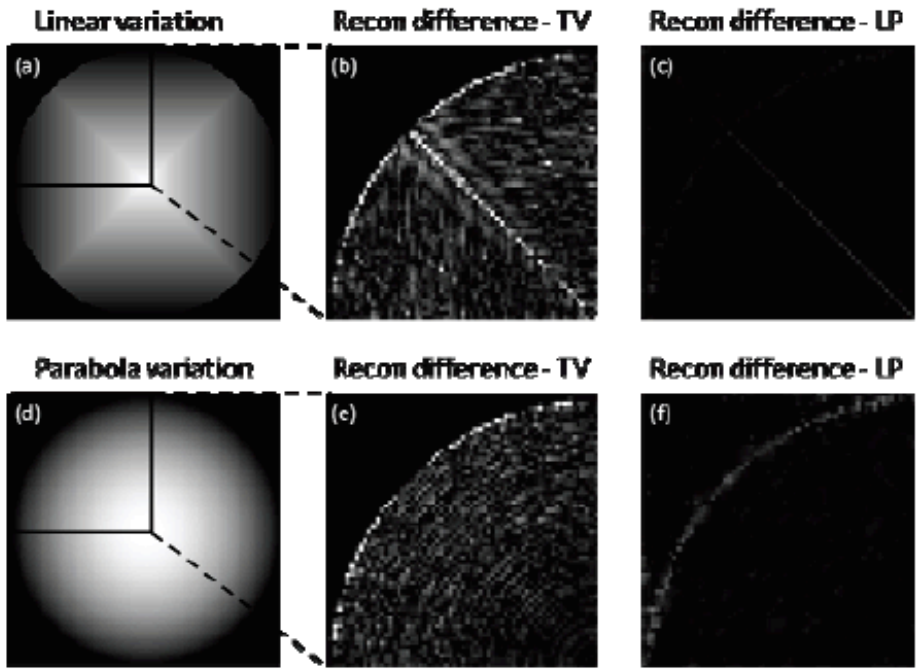


Fig.2 Comparison of LP and TV minimization for images with different non-uniformity: (a) original image with linear variation; (b – c) error images using TV or LP minimization; (d) original image with 2D parabola variation; (e – f) error images using TV or LP minimization.

Finally, an in-vivo spinal MRI dataset is used to test the proposed method. The data is acquired using a 4-channel linear array. The coil sensitivity creates a nonuniform weighting in the image. In this experiment, the image size is 128*128, sixty radial k-space lines, which is 40.8% of full k-space data, are used in the reconstruction.

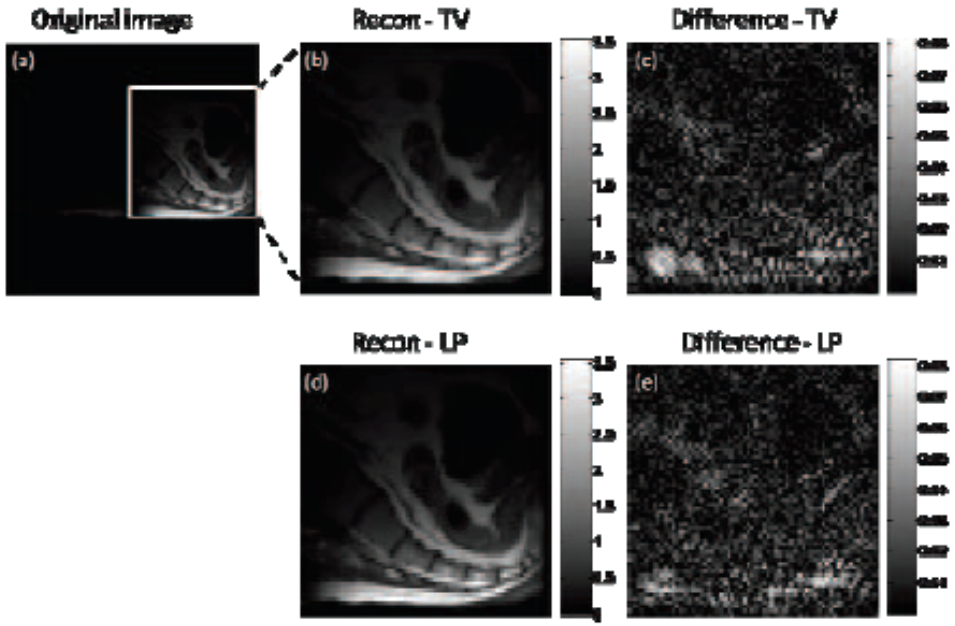


Fig.3 Image reconstruction in the in-vivo MRI spinal array experiment. (a) reference image reconstructed using full k-space data; (b) reconstruction using the TV minimization; (c) the corresponding error image; (d) reconstruction using the LP minimization; and (e) the corresponding reconstruction error image.

# REFERENCE-DRIVEN MR IMAGE RECONSTRUCTION WITH SPARSITY AND SUPPORT CONSTRAINTS

*Xi Peng*[*†], *Hui-Qian Du*[⋆†], *Fan Lam*[†], *S. Derin Babacan*[†] *and Zhi-Pei Liang*[†]

[*] School of Electronic Information, Wuhan University
[⋆] School of Information and Electronics, Beijing Institute of Technology
[†] Department of Electrical and Computer Engineering, University of Illinois at Urbana-Champaign

The signal acquisition scheme for MRI can be expressed as

$$s(\mathbf{k}) = \int \rho(\mathbf{r}) e^{-2\pi \mathbf{k}\cdot\mathbf{r}} d\mathbf{r}, \qquad (1)$$

prior to the injection of a contrast agent. This pre-injection image captures the underlying anatomical structure and can be used to construct a generalized series (GS) for reconstruction of the contrast-enhanced images with a small number of measurements [1]. Using

## 2.1. Proposed Model

We propose to model the target image as follows:

$$\rho(\mathbf{r}) = \sum_n c_{\mathrm{gs}}(n)\psi_{\mathrm{gs}}(n,\mathbf{r}) + \sum_{m\in\Omega} c_{\mathrm{w}}(m)\psi_{\mathrm{w}}(m,\mathbf{r}) + \sum_{l\in\Theta} c_{\mathrm{new}}(l)\psi_{\mathrm{new}}(l,\mathbf{r}) \qquad (3)$$

where $\psi_{\mathrm{gs}}$ are the GS basis functions, $\psi_{\mathrm{w}}$ are the wavelet basis functions, and $\psi_{\mathrm{new}}$ are the pixel indicator functions (the Dirac delta functions in the continuous case or the Kronecker delta functions in the discrete case); $c_{\mathrm{gs}}, c_{\mathrm{w}}, c_{\mathrm{new}}$ are the corresponding coefficients; $\Omega$ is the set of indexes of the selected wavelet basis functions and $\Theta$ is the set of indexes of the selected pixel indicator functions. The index set $\Omega$ represents the spectral support constraint and $\Theta$ often represents spatial support constraint (defining a region of interest).

The GS basis, $\psi_{\mathrm{gs}}(n,\mathbf{r})$, is given by $I_{\mathrm{ref}}(\mathbf{r})e^{i2\pi n\Delta\mathbf{k}\cdot\mathbf{r}}$, where $I_{\mathrm{ref}}$ is a given reference image. This set of basis is used to absorb general contrast variations between the reference image and the target image. In this work, we employ a low-order GS model, i.e., GS coefficients that correspond to low frequency components. While low-order GS model is effective in capturing large, low frequency contrast changes, it is not efficient for modeling localized contrast changes. The second term of the proposed model is introduced to address this deficiency of the low-order GS model through the use of wavelet basis which will capture the residual left by the low-order GS model. This partial set of wavelet basis functions is selected from a full wavelet basis based on prior information. Specifically in this work, a wavelet transform is applied to the reference image, and basis functions with large coefficients are selected. Other sparse

$$\underset{\mathbf{c}_{gs},\mathbf{c}_w,\mathbf{c}_{new}}{\operatorname{argmin}} \frac{1}{2}\|\mathbf{F}(\Psi_{gs}\mathbf{c}_{gs}+\Psi_w\mathbf{c}_w+\Psi_{new}\mathbf{c}_{new})-\mathbf{d}\|_2^2 + \lambda_1\|\mathbf{c}_w\|_1+\lambda_2\|\Psi_{new}\mathbf{c}_{new}\|_{TV} \quad (4)$$

where $\Psi_{gs}, \Psi_w$, and $\Psi_{new}$ are matrix operators whose columns are $\psi_{gs}$, $\psi_w$ and $\psi_{new}$ respectively. Thus, $\Psi_{new} = \mathbf{I}$. $\mathbf{c}_{gs}$, $\mathbf{c}_w$, $\mathbf{c}_{new}$ are the corresponding coefficient vectors. $\lambda_1$ and $\lambda_2$ are regularization parameters. $\|\cdot\|_{TV}$ is the discretized total-variation opera-

Equation (4) can be rewritten as:

$$\underset{\mathbf{c}}{\operatorname{argmin}} \frac{1}{2}\|\mathbf{F}\Psi\mathbf{c}-\mathbf{d}\|_2^2 + f(\mathbf{c})$$

where $\Psi = [\Psi_{gs}\ \Psi_w\ \Psi_{new}]$, $\mathbf{c} = \begin{bmatrix} \mathbf{c}_{gs} \\ \mathbf{c}_w \\ \mathbf{c}_{new} \end{bmatrix}$.

For the anisotropic total-variation case, we have:

$$f(\mathbf{c}) = \|\mathbf{B}\mathbf{c}\|_1$$

where

$$\mathbf{B} = \begin{bmatrix} \lambda_1\mathbf{H}_w \\ \lambda_2\mathbf{D}_1\mathbf{H}_{new} \\ \lambda_2\mathbf{D}_2\mathbf{H}_{new} \end{bmatrix}, \mathbf{H}_w\mathbf{c} = \mathbf{c}_w, \mathbf{H}_{new}\mathbf{c} = \mathbf{c}_{new}.$$

For the isotropic total-variation case, we apply the operator splitting method [13] to Eq. (4):

# 3. EXPERIMENTS

the target image. The global contrast variation is captured by a set of $16 \times 16$ low-order GS basis functions. Since accurate registration is essential for GS modeling, the reference image is registered to the target image before the GS basis is constructed. This is done using

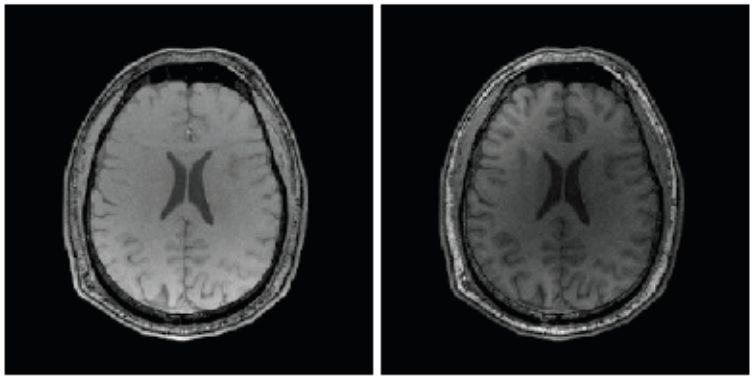

(a) (b)

**Fig. 1.** a) Reference image used to build into the GS basis and b) the target image.

proposed model. 18000 (out of 65536) wavelet basis functions, two-level Haar wavelet is used here, are selected to capture the localized changes. In addition, a narrow dark line was added to the target image, mimicking the effect of a needle being inserted into the object (e.g., in interventional MRI). The deformation of the surrounding tissue can be captured by the wavelet functions and the pixel/voxel indicator functions. The support of the needle is shown in Fig. 2a as a white rectangular. Variable density random sampling pattern was used for data acquisition [3].

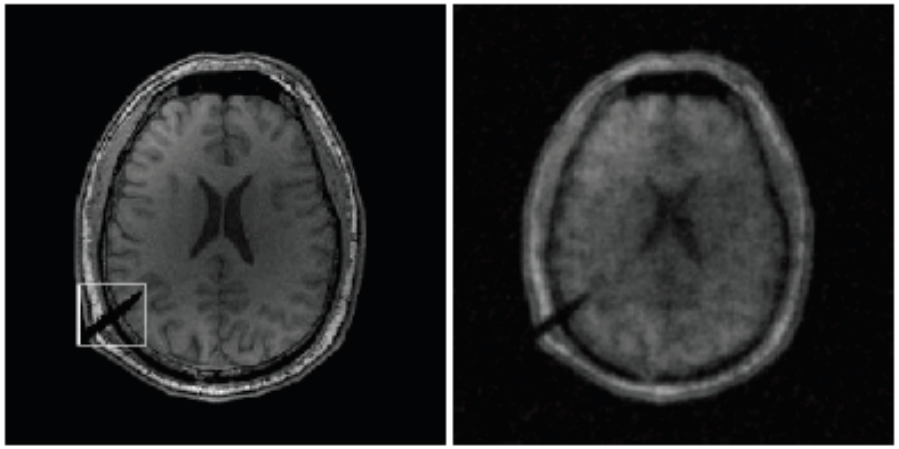

(a) True (b) CS (TV)

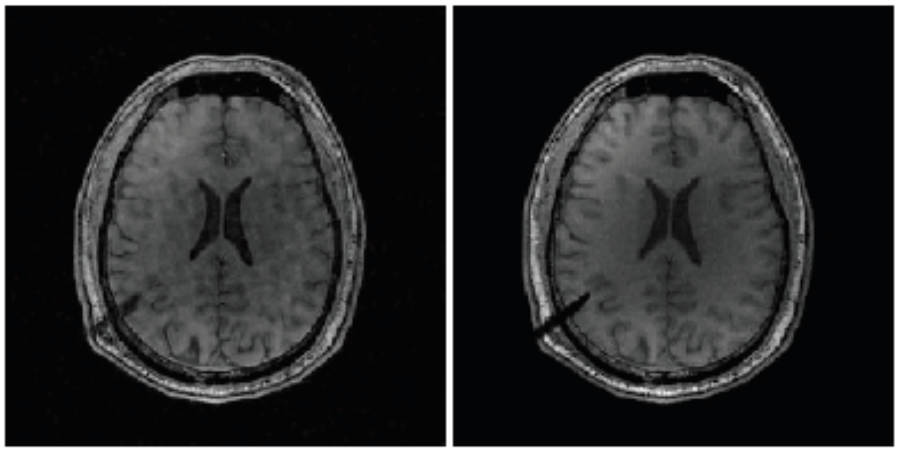

(c) Diff. CS (TV) (d) Proposed

The proposed method was compared with two conventional CS-based reconstruction schemes. The first one uses TV regularization on the entire image (CS (TV)), and the second uses TV regularization on the difference of the reference image and the target image (Diff. CS (TV)). The anisotropic total-variation is used in all the

$$e = \frac{\|\hat{\rho} - \rho_0\|_2}{\|\rho_0\|_2},$$

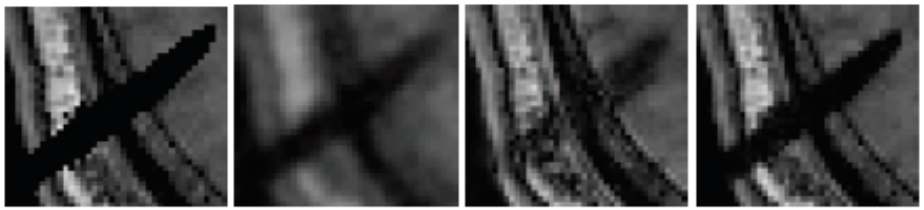

(e) True (f) CS (TV) (g) Diff.CS (TV) (h) Proposed

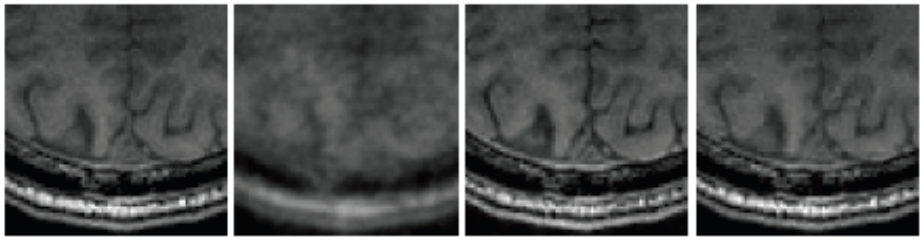

(i) True (j) CS (TV) (k) Diff.CS (TV) (l) Proposed

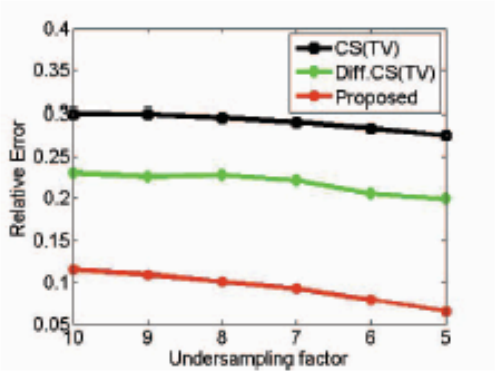


**Fig. 3**. Reconstruction errors of three different methods.

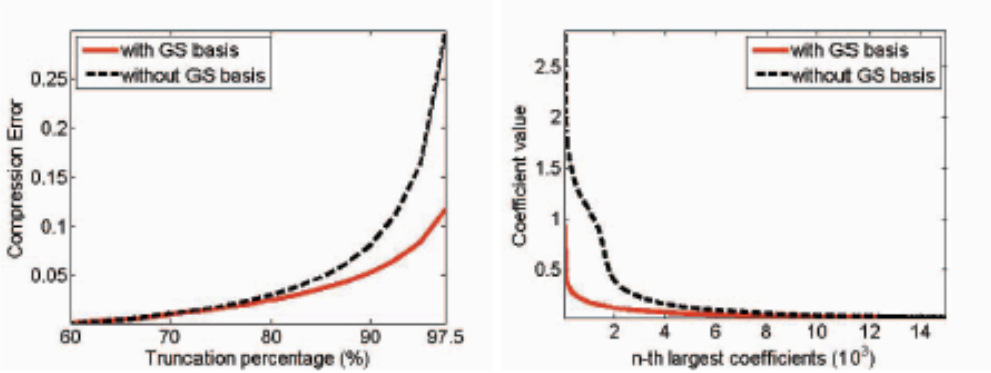


(a) (b)

**Fig. 4**. Improved compressibility using GS model. a) Compression error. b) Wavelet coefficients in a descendent order.

# COMPRESSED SENSING BASED INTENSITY NON-UNIFORMITY CORRECTION

*Snehashis Roy, Aaron Carass, and Jerry L. Prince*

Image Analysis and Communications Laboratory, Electrical and Computer Engineering,
The Johns Hopkins University

bias from many images simultaneously. In this work, however, we propose a non-parametric compressed sensing based intensity non-uniformity correction (CSI-NC) approach that does not have any explicit smoothness model on the estimated field and does not require many images, thus being more versatile and applicable to situations where the actual IIH is not smooth, e.g. in 7T images.

$$\hat{\mathrm{x}} = \underset{\mathrm{x}}{\operatorname{argmin}}\{||\mathrm{y} - \Phi\mathrm{x}||_2^2 + \lambda||\mathrm{x}||_1\},$$

## 2.2. Patch Based Correction

Assume the MR image is partitioned into $p \times q \times r$ patches. the bias field is not globally smooth, then we can assume th it is at least uniform over a small image patch. Let $d = pq$ thus each patch can be thought of as a $d \times 1$ vector. Assumi that the gain field is multiplicative, each image patch $\mathrm{y}_k$ $\mathbb{R}^d$, $k \in \Omega$, can be written as,

$$\mathrm{y}_k = g_k \mathrm{y}_k^\star + \eta_k,\ g_k > 0 \qquad ($$

Here, $\Omega$ is the image domain, $\mathrm{y}_k^\star$ is the inhomogeneity free image patch, $g_k$ is the bias field for $k^{th}$ location, and $\eta$ is the image noise. For further analysis, for simplicity we assume that $\eta_k = 0, \forall k$.

Specifically, consider the sparse representations of $\mathrm{y}_k$ and $\mathrm{y}_k^\star$ as $\mathrm{x}_k$ and $\mathrm{x}_k^\star$, respectively. Then Eqn. 3 gives,

$$\hat{\mathrm{x}}_k = \underset{\mathrm{x}}{\operatorname{argmin}}\{||\mathrm{y}_k - \Phi\mathrm{x}||_2^2 + \lambda||\mathrm{x}||_1\}, \mathrm{x} \geq 0 \qquad (5)$$

$$\hat{\mathrm{x}}_k^\star = \underset{\mathrm{x}}{\operatorname{argmin}}\{||\mathrm{y}_k^\star - \Phi\mathrm{x}||_2^2 + \lambda^\star||\mathrm{x}||_1\}, \mathrm{x} \geq 0 \qquad (6)$$

Now if $\mathrm{y}_k = g_k \mathrm{y}_k^\star$, Eqn. 5 gives,

$$\begin{aligned} \hat{\mathrm{x}}_k &= \underset{\mathrm{x}}{\operatorname{argmin}}\{||g_k\mathrm{y}_k^\star - \Phi\mathrm{x}||_2^2 + \lambda||\mathrm{x}||_1\}, \\ \Rightarrow \hat{\mathrm{x}}_k &= \underset{\mathrm{x}}{\operatorname{argmin}}\left\{||\mathrm{y}_k^\star - \Phi\frac{\mathrm{x}}{g_k}||_2^2 + \frac{\lambda}{g_k}\left|\left|\frac{\mathrm{x}}{g_k}\right|\right|_1\right\}, \end{aligned} \qquad (7)$$

By appropriate conditions on $\Phi$ as described earlier, and choosing $\lambda = g_k\lambda^\star$, Eqn. 7 and Eqn. 6 give $\hat{\mathrm{x}}_k = \hat{\mathrm{x}}_k^\star g_k$. Thus, an appropriate estimator of $g_k$ is given by,

$$g_k = \frac{||\hat{\mathrm{x}}_k||_1}{||\hat{\mathrm{x}}_k^\star||_1}. \qquad (8)$$

### 2.3. Choice of $\hat{\mathrm{x}}_k^\star$ and $\Phi$

Eqn. 8 suggests that in an ideal situation, if two inhomogeneity free patches $\hat{\mathrm{y}}_i$ and $\hat{\mathrm{y}}_j$ are of same the tissue and have the same intensity, then $\hat{\mathrm{x}}_i^\star = \hat{\mathrm{x}}_j^\star$ and $g_i \propto ||\hat{\mathrm{x}}_i||_1$, *i.e.*, the $L_1$ norm of the sparse representation gives the relative amount of gain field for the same tissue.

For a particular $k$, $\hat{\mathrm{x}}_k^\star$ can be found using a prior information about the tissue classes, which can be obtained from a segmentation of the image. The image being already corrupted with IIH, we only need an approximate segmentation of the image. In our experiments, we have used an atlas based segmentation called TOADS [16] that uses a probability atlas

Here we note that all images are normalized, so that their WM peaks have the same value. The final inhomogeneity field becomes blocky because there is no explicit smoothness criterion on the image model. As a post-processing step, we smooth the field by a Gaussian filter with size $\sigma$, that we estimate based on phantom validation, described in the next section. The filter also smooths out bad estimates of $\hat{\mathrm{x}}_k$'s near the tissue boundaries.

The compressed sensing literature suggests that a good choice of $\Phi$ is a random matrix. For our experiments, we generate $\Phi$'s from a uniform distribution once.

The algorithm is described as follows,

1. Partition the image into patches $\mathrm{y}_k$, $k \in \Omega$ of size $p \times q \times r$. In our experiments, $p = q = r = 3$. Generate a random $d \times N$ matrix $\Phi$. In our experiments, we arbitrarily select $N = 1000$.

2. Find an approximate segmentation of the image using TOADS and compute the mean $\mathrm{y}^{(l)}$'s that represents the $l^{th}$ class, $l = 1, \ldots, 4$. Find the corresponding $\hat{\mathrm{x}}^\star(l)$'s using $\Phi$ in Eqn. 5.

3. For each $k$, find the type of the tissue $l_0 \in \{1, \ldots, 4\}$ that $\mathrm{y}_k$ belongs to. If there is more than one tissue type in $\mathrm{y}_k$, we choose the dominant one for simplicity. Then $\hat{\mathrm{x}}_k^\star = \hat{\mathrm{x}}^\star(l_0)$

4. Find the sparse representation of $\mathrm{y}_k$ as $\hat{\mathrm{x}}_k$ from Eqn. 5. We use $\lambda = 0.5$.

5. Find the gain field $g_k$ using $\hat{\mathrm{x}}_k$ and $\hat{\mathrm{x}}^\star(l_0)$ using Eqn. 8.

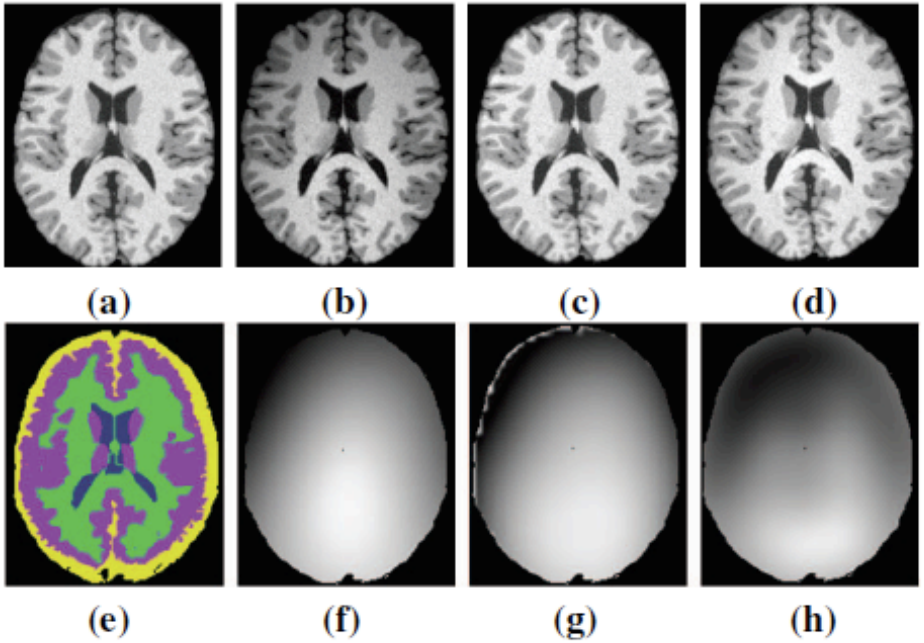


**Fig. 3.** **(a)** Original inhomogeneity free image, **(b)** corrupted by 20% INU as described in [17], **(c)** N3 corrected image, **(d)** CSI-NC corrected image, **(e)** crude segmentation by TOADS [16] that is used to find $\hat{x}^{\star}(l)$ described in Sec. 2.3, **(f)** true inhomogeneity field "C", **(g)** N3 inhomogeneity field, **(h)** CSI-NC field, smoothed by a Gaussian filter of size $\sigma = 10$mm.

fashion in a high-dimensional parameter space. Instead, we employ a patch based method. We use both CSI-NC and N3 on Philips 7T MPRAGE (magnetization prepared rapid gradient echo) and FLAIR (fluid attenuated inversion recovery) images, $256 \times 320 \times 320$ volumes, 0.70mm isotropic.

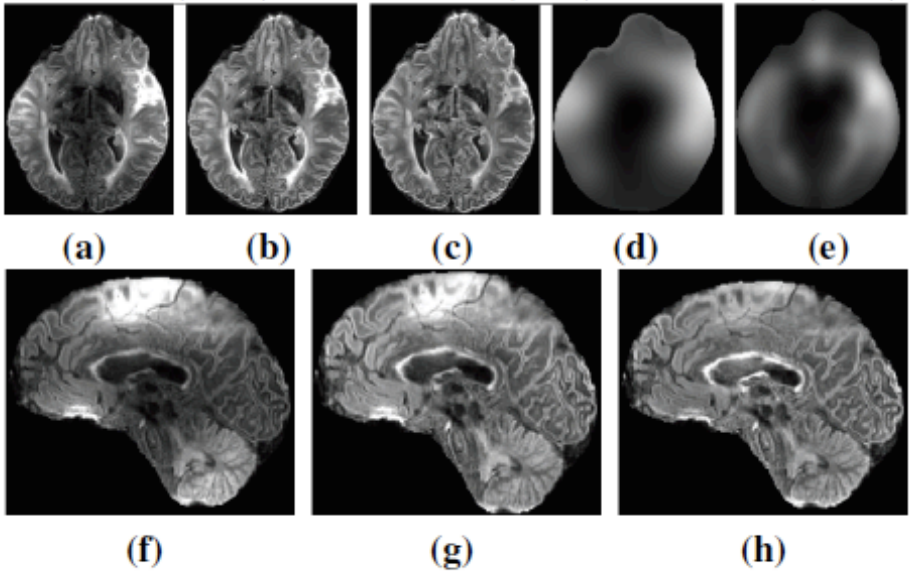


**Fig. 4.** **(a)** Original 7T FLAIR image, **(b)** N3 corrected FLAIR, **(c)** CSI-NC corrected image, **(d)** N3 field, **(e)** smoothed field from CSI-NC, smoothed by Gaussian filter of size 10mm, **(f)** a sagittal view of the original FLAIR, **(g)** sagittal view of N3 corrected image, **(h)** sagittal view of CSI-NC corrected image. As N3 assumes an underlying smoothness model on the inhomogeneity, small localized inhomogeneity that are present in small tissue structures are not corrected.

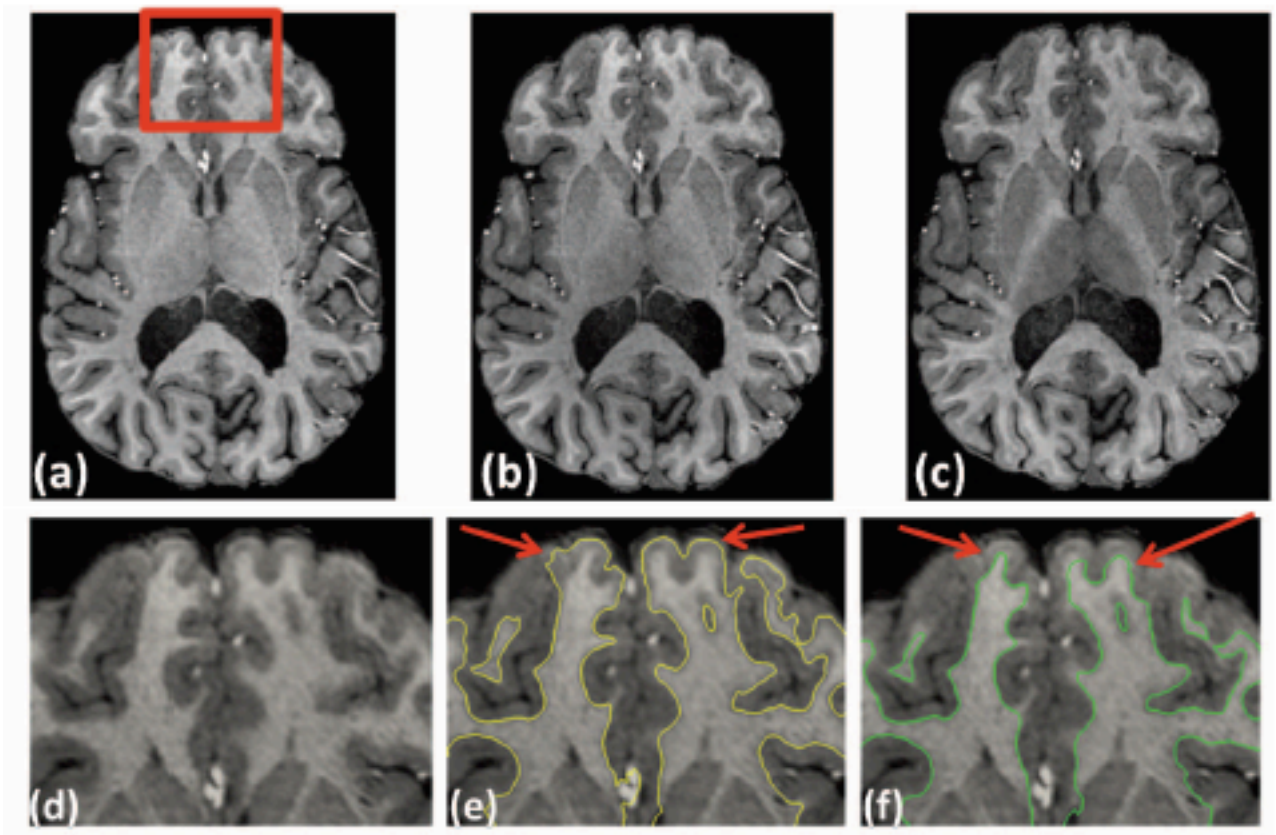


**Fig. 5.** (**a**) Original 7T MPRAGE image, (**b**) correction by N3, (**c**) correction by CSI-NC, (**d**) a zoomed in version of the original MPRAGE, (**e**) inner cortical surface [18] generated from the N3 corrected image (yellow) and (**f**) from CSI-NC corrected image (green), overlaid on the original MPRAGE.